Fine Structure Constant Variation

by

Hurum Maksora Tohfa

Submitted in Partial Fulfillment of the Requirements

for the Degree of BA (Honors) in Physics

Advised by

Professor Daniel Grin

Department of Physics

Bryn Mawr College

Bryn Mawr, PA

Spring 2022

CONTENTS

LIST OF FIGURES

ABSTRACT

In some extensions of the standard model of particle physics, the values of the fundamental coupling constants could vary in space and time. In some string inspired scenarios, the couplings relate to the size of extra dimensions. Some recent observations of QSO hinted at possible time and spatial variation of the fine structure constant. We analyzed the Bekenstein-Sandvik-Barrow-Magueijo (BSBM) model which posits the existence of a cosmological scalar field and allows the field and the fine structure constant to evolve with the expansion of the universe as well as the string inspired model runaway dilaton. We explore which models are consistent with the CMB anisotropies measured by Planck and quasar observations.

I. INTRODUCTION

As the unification of fundamental forces of nature only seem to exist in finite form if there are more than our familiar four dimensions, it is likely that our familiar natural constants defined in higher dimension and the three dimension projection of it that we are familiar with is not constant. This idea has inspired an increasing interest in nature's fundamental constants and their variation. This idea was first introduced by Dirac as he showed the numerical coincidence that $3e^2/(Gm_pm_e) \simeq tm_ec^3/e^2$ where e is the charge of electron, m_p is the mass of proton, m_e is the mass of electron, G is our known gravitational constant and c is the speed of light. He suggested fundamental constants such as G, Planck's constant, $\hbar$, m_e etc are dynamic parameters that vary as a function of time [12]. While these specific scalings have been ruled out on anthropic grounds, it inspired a class of theories for the dynamic fine structure constant, α ($\alpha = \hbar c/e^2$) which tells us how photons and electromagnetic particles interact in space [2].

Another significant motivation for studying fine structure constant variation comes from recent observation of CMB polarization and measurements of primordial lights from measurements of distant supernovae, Sloan Digital Sky Survey, Planck, COBE in recent years. These observations has also strengthened our understanding of early universe cosmology such as inflation, recombination etc. Upcoming observational data from Simons Observatory, CMB S4, BICEP/KECK and other next generation experiments may show deviation

from standard model since our current standard model cannot explain the phenomena we observe in our universe, and probe physics of neutrinos, number of their effective species, and deviations from general relativity (GR) at cosmological scales[19, 20].

Some recent observations has shown a possibility of α variation. In particular, the absorption spectra of quasars, showed a possibility of cosmological time and spatial variation on the fine structure constant [24, 30, 36, 38, 39]. For this work, we use Quasar observation data test for the first time well-modulated models of α variation using CMB radiation. We base our work on Ref. [17]'s model independent fundamental constant variation using CMB polarization and temperature anistropies to explicitly constrain our models for consistent fine structure constant variation across redshift 3 (Quasar observation) up to and including decoupling and matter-radiation equality till redshift 4000.

For this work, we use two theoretical models that can that incorporate α as a dynamical constant: Bekenstein's α variation model and Damour's Runaway Dilaton Model. Beckenstein's α variation model is the simplest U(1) gauge invariant model which has a conservation law where the conserved charge is proportional to e. This allows electric charge to vary in space without throwing away charge conservation. The full theory, Bekenstein-Sandvik-Barrow-Magueijo (BSBM) model, and some extensions of BSBM that considers more complicated scalar field couplings and potentials allow us to predict α across time and space. On the other hand, the runway dilaton model also allows conservation of Maxwell's equation but it also gives us a direct conformal coupling to matter. The strong coupling of the associated scalar field in this model allow variation on the fine structure constant.

We explore these models to find suitable families of parameters that allow fine structure to vary across time. Since this work relies on developing novel numerical techniques to understand physical phenomena, it is important to understand both the physical theories, and background for the used computational methods. We will be discussing them separately in the following sections.

II. IMPORTANT PHYSICAL BACKGROUND

In this section, we give an overview on the relevant scientific background to understand the cosmology of fine structure variation. In particular, we will talk about the Quasar Absorption Spectra which motivated this work, cosmology of the early universe and discuss
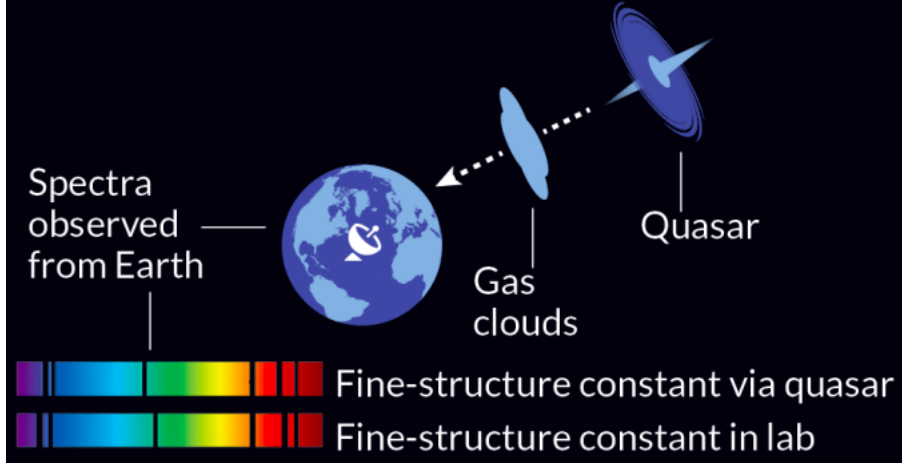
Figure 1: Quasar Observation as seen from earth. Image Credit: Science News

.

the relevant formalism, the cosmic microwave background radiation and other processes that took place in the early universe which led us to constrain fine structure constant using this particular data. We also discuss the BSBM Model, the Runaway Dilaton Model associated with the fine structure constant variation.

A. Quasar Absorption Spectra

Atoms absorb electromagnetic radiations at different wavelengths. The wavelengths of these electromagnetic radiation (light) shows up at different color of light when we observe the atom's power spectra. Quasars are strong sources whose light would be absorbed by influencing gas. So, their spectra can be used as probes of varying α.

When we observe Quasar from the earth, we see atoms and ions which absorb light at different characteristic wavelengths (colours) determined by the type of ion and the position of sight (redshift). The colors absorbed in an intervening gascloud depend on the redshift and the ions present. It is related to fine structure constant by $\Delta\lambda \propto \alpha^2$. Recent observation of Quasi-Stellar Object (QSO) has shown deviation from laboratory observed value of the fine structure constant by 3σ.

B. The Early Universe, its evolution

The beginning of the space-time started from a singularity known as Big Bang. Right after the big bang, the universe expanded exponentially instantly. This process is inflation. The universe has been expanding ever since. It is widely accepted the universe is flat and spatially homogeneous and isotropic. For an expanding homogeneous and isotropic universe we use a spacetime metric that is maximally symmetric when we look at three dimensional slices. We can consider our spacetime then as $\mathbf{R} \times \Sigma$ where Σ is a maximally symmetric manifold. Then the spacetime metric is:

$$ds^2 = -dt^2 + R(t)d\sigma^2, \tag{1}$$

Here R(t) is a scale factor and $d\sigma$ is the metric on Σ. It can be expressed as:

$$d\sigma^2 = \gamma_{ij}(u)\mathrm{d}u^i \ \mathrm{d}u^j, \tag{2}$$

The u^i are spatial coordinates and γ_{ij} is a maximally symmetric three dimensional metric. The fact that the dt^2 is independent of spatial coordinate and there is no dudt term means that they are comoving coordinates. This is set up this way because the universe can look isotropic only to a comoving observer. The fact that we are not moving with respect to cosmic expansion due to earth's motion causes us to see a dipole anistropy in cosmic microwave background radiation due to Doppler effect. Using ansatz of a static, spherically symmetric solution and applying spherical symmetry we can solve for the Ricci tensor and yield the metric on three surface Σ,

$$d\sigma^2 = \frac{\mathrm{d}\bar{r}^2}{1 - k\bar{r}^2} + \bar{r}^2 d\Omega^2. \tag{3}$$

Here $\bar{r}$ is the comoving radial coordinate, $d\Omega^2 = d\theta^2 + sin^2\theta d\phi^2$ and k is the value of curavture. The curvature value corresponds of curvature on Σ as one would expect. We can also substitute the R(t) with a dimensionless scale factor defined as:

$$a(t) = \frac{R(t)}{R_0}, \kappa = \frac{k}{R_0}. \tag{4}$$

Then the spacetime metric can be rewritten as below:

$$ds^2 = -\mathrm{d}t^2 + a^2(t)\left[\frac{\mathrm{d}r^2}{1 - \kappa r^2} + r^2 d\Omega^2\right]. \tag{5}$$

To understand the scale factor a(t), we need to plug a(t) to Einstein's equation:

$$R_{\mu\nu} = 8\pi G \left(T_{\mu\nu} - \frac{1}{2} g_{\mu\nu} T \right), \tag{6}$$

where $R_{\mu\nu}$ is Ricci Tensor, $g_{\mu\nu}$ is metric tensor and $T_{\mu\nu}$ is energy momentum tensor. Now for a universe filled with perfect fluid matter and energy, the energy-momentum tensor is just:

$$T_{\mu\nu} = \begin{pmatrix} \rho & 0 & 0 & 0 \\ 0 & p/c^2 & 0 & 0 \\ 0 & 0 & p/c^2 & 0 \\ 0 & 0 & 0 & p/c^2 \end{pmatrix}. \tag{7}$$

Now, choosing an equation of state $p = w\rho$ makes the energy-conservation equation:

$$\frac{\dot{\rho}}{\rho} = -3(1+w)\frac{\dot{a}}{a} \tag{8}$$

Here, w is a constant. For different value of w depending on whether we are in a matter dominated or radiation dominated or vacuum dominated universe, we get a different relationship between the scale factor and the density. The scale factor is related to the density as the equation of state power. What it means is that, for a matter dominated universe, since matter omits zero pressure, we can set w to 0. Then matter density, $\rho_m \propto a^{-3}$. On the other hand, for a radiation dominated universe, radiation can be thought of as electromagnetic radiation as well as relativistic particles that move so fast that they are not distinguishable from photons. Using the fact that $T_{\mu\nu}$ can be expressed in terms of field strength and an isotropic gas of relativistic particle is a perfect fluid, we can get the equation of state as $P_r = \frac{1}{3}\rho_r$, w= 1/3. Then the solution to Eq. (9) becomes $\rho_r \propto a^{-4}$. As we can see, the energy density in radiation falls off slightly faster than energy density in matter. As a result, the radiation energy density is less than matter energy density (almost $\sim 10^3$ times). However, in early times, the universe was denser and radiation dominated. We therefore must account radiation density when modeling an expanding universe at early times.

The universe takes form of a perfect fluid when we consider vacuum energy. Which gives us solution to equation (9) as $\rho_\Lambda \propto a^0$. Which means as the universe expands, the vacuum energy win over the other two terms in the expansion equation.

Now going back to Einstein's Eq. 9, for $\mu\nu$=00, we get:

$$-3\frac{\ddot{a}}{a} = 4\pi G(\rho + 3p). \tag{9}$$

Eq. (10) gives the second derivative of expansion. Since the discovery of Hubble parameter, cosmologists have looked for evidence for the expansion of the universe to slow down due to gravity. However, in 1998, two distinct studies on distant Type Ia supernovae gave evidence that the expansion rate of the universe has been accelerating [26, 34] . Subsequent observations, including more detailed studies of supernovae and independent evidence from clusters of galaxies, large-scale structure, and the cosmic microwave background (CMB), confirmed and firmly established this remarkable finding [15]. This presented two possible explanations: 1) 75 percent of the energy density of the universe has a large negative pressure called dark energy, 2) general relativity breaks down on cosmological scales. Now there are different possibilities for dark energy models. One is vacuum energy. General covariance requires that the stress-energy of the vacuum takes the form of a constant times the metric tensor. Which makes the pressure equal to negative density. However, it also means that vacuum energy is mathematically just a constant. Attempts to calculate vacuum energy density has given a diverse set of results. For each mode of a quantum field there is a zero-point energy $\hbar\omega/2$, then the density is :

$$\rho_{\text{VAC}} = \frac{1}{2} \sum_{\text{fields}} g_i \int_0^\infty \sqrt{k^2 + m^2} \frac{d^3k}{(2\pi)^3} \simeq \sum_{\text{fields}} \frac{g_i k_{\text{max}}^4}{16\pi^2}. \qquad (10)$$

Here g_i accounts for degrees of freedom and the sum runs over all quantum fields (quarks, leptons, gauge fields, etc). Here k_{max} is an imposed momentum cutoff, because the sum diverges quartically. This creates a problem because if the energy density contributed by just one field is to be at most the critical density, then the cutoff k_{max} must be ¡ 0.01 eV. This energy scale is extremely small. If we compare it to Planck energy scale where we expect quantum field theory in a classical spacetime metric to break down, the zero-point energy density would exceed the critical density by 120 orders of magnitude.

To solve the dark energy problem, we can introduce a new degree of freedom in the form of a scalar field to make the dark energy dynamical [14, 40, 41]. Here we also review the scalar field dynamics using equations of Chameleon theory because of its structural similarity with BSBM. Chameleon here refers to the ϕ field. In high density regions, the scalar field blends with its environment and becomes essentially invisible to searches for Equivalence Principle violations. The action for the field using scalar-tensor theory [5] is:

$$S = \int d^4x \sqrt{-g} \left[\frac{M_P^2}{2} R - \frac{1}{2} \nabla_\mu \phi \nabla^\mu \phi - V(\phi) \right] + \int d^4x \mathcal{L}_{\text{m}} \left(\tilde{g}_{\mu\nu} \right), \qquad (11)$$

where $S_{\mathrm{m}} = \int d^4 x \mathcal{L}_{\mathrm{m}} (\tilde{g}_{\mu\nu}) = \int d^4 x \sqrt{-\tilde{g}} \hat{\mathcal{L}}_{\mathrm{m}} (\tilde{g}_{\mu\nu})$. This describes a canonically normalized scalar field with some potential $V(\phi)$. This field is coupled with matter through the Jordan frame metric:

$$\tilde{g}_{\mu\nu} = A^2(\phi) g_{\mu\nu}. \tag{12}$$

This non-minimal coupling described by the coupling function $A(\phi)$ results in deviations from general relativity. Varying ϕ with respect to the scalar field gives [using $\delta\phi(x)/\delta\phi(y) = \delta^4(x-y)$]:

$$\frac{\delta S}{\delta\phi(y)} = \int d^4 x \sqrt{-g} \left[\Box\phi(x) - V' \right] \frac{\delta\phi(x)}{\delta\phi(y)} + \frac{\delta S_{\mathrm{m}}}{\delta\phi(y)}. \tag{13}$$

The last term of the right hand side can be written as below using $T_{\mu\nu} \equiv -\frac{2}{\sqrt{-g}} \frac{\delta S}{\delta g^{\mu\nu}}$

$$\frac{\delta S_{\mathrm{m}}}{\delta\phi(y)} = \sqrt{-g} \frac{A'}{A} T^{\mathrm{m}}_{\mu\nu} g^{\mu\nu} \frac{\delta\phi(x)}{\delta\phi(y)}. \tag{14}$$

Then, we can rewrite Eq. (15) with $T^{\mathrm{m}} \equiv T^{\mathrm{m}}_{\mu\nu} g^{\mu\nu}$:

$$\frac{\delta S}{\delta\phi(y)} = \sqrt{-g} \left(\Box\phi - V' \right) + \sqrt{-g} \frac{A'}{A} T^{\mathrm{m}}_{\mu\nu} g^{\mu\nu} = 0,$$
$$\Box\phi = V' - \frac{A'}{A} T^{\mathrm{m}}. \tag{15}$$

Then for non-relativistic matter ($T^{\mathrm{m}} \approx -\rho_{\mathrm{m}}$) and effective potential $V'_{\mathrm{eff}} = V' + \frac{A'}{A} \rho_{\mathrm{m}}$, this reduces to $\Box\phi = V'_{\mathrm{eff}}$. On the other hand, the d'Alembertian can be rewritten as:

$$\Box\phi = g^{\mu\nu} \nabla_\mu \left(\nabla_\nu \phi \right) = \nabla_\mu \left(\partial^\mu \phi \right),$$
$$= \partial_\mu \left(\partial^\mu F_\phi \right) + \Gamma^\mu_{\mu\lambda} \left(\partial^\lambda \phi \right), \tag{16}$$
$$= -\partial_0^2 \phi - 3H \partial_0 \phi.$$

Then the equation of motion for the scalar field becomes:

$$\ddot{\phi} + 3H\dot{\phi} + V'_{\mathrm{eff}} = 0. \tag{17}$$

Instead of varying the action with respect to ϕ, if we vary the action with $g^{\mu\nu}$, the stress-energy tensor project onto time-direction of fluid rest frame. The pressure and density then takes the form below [26]:

$$p = \frac{\dot{\phi}^2}{2} + V(\phi), \tag{18}$$

$$\rho = \frac{\dot{\phi}^2}{2} - V(\phi). \tag{19}$$

Scalar-field dark energy can be described by the equation-of-state parameter similar to Eq. (9) as:

$$w = \frac{\dot{\phi}^2/2 - V(\phi)}{\dot{\phi}^2/2 + V(\phi)} = \frac{-1 + \dot{\phi}^2/2V}{1 + \dot{\phi}^2/2V}. \tag{20}$$

For a slowly evolving scalar field ($\dot{\phi}/2V << 1$), we get a slowly varying vacuum energy with w = -1. On the other hand, from our previous discussion of expanding universe, combining Eq. (10) and Eq. (11) from our above discussion, it can be shown that:

$$\left(\frac{\dot{a}}{a}\right)^2 = 4\pi G\rho - \frac{\kappa}{a^2}. \tag{21}$$

This equation is known as the Friedmann equation. It is perhaps one of the most important equation in cosmology. The left hand side of the equation tells us whether and how much the universe is expanding as a function of time denoted by Hubble parameter. The right hand side constitutes of everything that makes up our universe like matter, radiation, and any other forms of energy. This seemingly simple equation connects matter and energy to expansion rate of the universe at any given time and help us understand growth and formation of the large scale structures (by adding perturbations to the density).

We can rewrite the Friedmann equation to get density parameter, Ω in terms of H:

$$\Omega = \frac{\rho}{\rho_{\text{crit}}} = \frac{8\pi G}{3H^2}\rho. \tag{22}$$

As one can imagine for different type of energy density, $\rho_i = \rho_{i0}a^{-n-i}$ using are solutions to Eq. (9). Then for each energy density is we will have a corresponding Ω that is a dimensionless quantity and $\sum \Omega_i = 1$. But this is not the total density as we are only taking account of energy density. There is also curvature density which is $\Omega_c = 1 - \Omega$. Then we can finally write the Hubble parameter with our newly defined density parameters:

$$H^2(a) = H_0^2 \left(\Omega_m a^{-3} + \Omega_r a^{-4} + \Omega_k a^{-2} + \Omega_\Lambda\right). \tag{23}$$

Throughout this work, for our defined cosmological parameters, we use Hubble parameter today has value $H_0 \sim 70$ km s^{-1} Mpc^{-1} and determine the value of the density parameters using the luminosity-distance formula. These parameters can also be constrained using radiation that reaches us from big bang known as the Cosmic Microwave Background (CMB) Radiation.

For the last discussion of this section, we will relate redshift with our defined parameters as the data from Quasar we will be using are given as function of redshift. Now, consider a

photon which is known to have a metric ds = 0. Then the FRW metric tells us:

$$\int_{t_e}^{t_0} \frac{c}{a(t)} \mathrm{d}t = \int_0^{r_M} dr = r_M. \tag{24}$$

This can be written this in terms of wavelength:

$$\frac{\lambda_e}{a\left(t_e\right)} = \frac{\lambda_0}{a\left(t_0\right)}. \tag{25}$$

Using the above relation and definition of redshift, we get

$$a(t) = \frac{1}{1+z}. \tag{26}$$

We will be using this definition throughout this whole writing assuming the redshift is 0 today.

C. Decoupling and the CMB

Since the early universe was extremely dense and hot, all the matter is ionized and forms a plasma in which the photons are bound to move with the matter due to their scattering off free electrons. Even if the universe is initially largely homogeneous, quantum fluctuations are created. These fluctuations in the density of the universe are amplified by the action of gravity. It makes the region further denser. At this stage, the plasma was opaque to electromagnetic radiation as Thomson scattering of free electrons made the mean free path that each photon could travel before encountering an electron very short.

Now, as the universe expanded, the temperature cooled down. Once it has cooled sufficiently, and the energy level became stable enough for electrons to bond with protons for forming neutral atoms. This process is known as recombination. The process of recombination can be described using the Saha equation for a single hydrogen atom:

$$\frac{1 - X_{\mathrm{e}}}{X_{\mathrm{e}}^2} = \frac{t\sqrt{2}\zeta(3)}{\sqrt{\pi}} \eta \left(\frac{T}{m_{\mathrm{e}}}\right)^{3/2} \exp\left(\frac{13.6\mathrm{eV}}{T}\right). \tag{27}$$

Where X_e is the ionization fraction and η is the baryon to photon ratio.

Once the gas (previously what was plasma) became neutral, the photons that previously had a short mean free path are free to spread throughout the universe. The mean path for these photons then became much larger than the Hubble distance. It filled the universe with freely propagating photons with blackbody radiation of temperature $\sim 3000\mathrm{K}$. This process
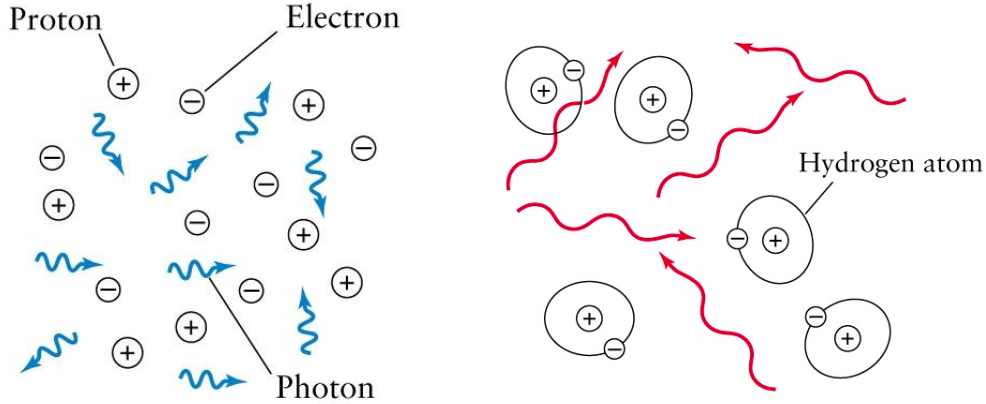
Figure 2: Hydrogen atom recombination in early universe as seen in Ref. [33]

.

took place about 375,000 years after the Big Bang (around redshift ~ 1100, 13.6 billion years ago). This isotropic radiation that spread throughout the universe can be detected on earth today as perfect blackbody radiation spectrum.

However, as the universe expanded the photons redshift. So, the temperature of the photons drop with the increase of the scale factor (a) introduced in previous section as $T \propto 1/a$. We can detect these photons today as the CMB.

The average temperature of CMB is 2.725K. However, in 1992, COBE satellite found fluctuation in temperature with a variation of $T \sim 10^{-5}$. We can write down a temperature function depending on its angular position in the sky. We can express this in terms of the spherical harmonics $Y_\ell^m(\theta, \phi)$, which form an complete, orthogonal basis for the space of functions on the sphere. Then we may find coefficients a_{lm} such that:

$$T(\theta, \phi) = \sum_{\ell m} a_{\ell m} Y_{\ell m}(\theta, \phi). \tag{28}$$

We can then define the angular power spectrum as: $\left\langle a_\ell^m \left(a_{\ell'}^{m'}\right)^* \right\rangle = \delta_{\ell \ell'} \delta_{mm'} C_\ell^{TT}$. We can therefore get an estimate of the power spectrum at some given value l as the average of over all modes as:

$$\hat{C}_\ell^{TT} = \frac{1}{2\ell + 1} \sum_{m=-\ell}^{\ell} |f_\ell^m|^2, \tag{29}$$

with an uncertainty of $\sqrt{2/(2\ell + 1)}$. This uncertainty is known as cosmic variance. This tells us how accurately can the spectra ultimately be measured.

Gravitational attraction tends to increase the density in dense regions, but the radiation
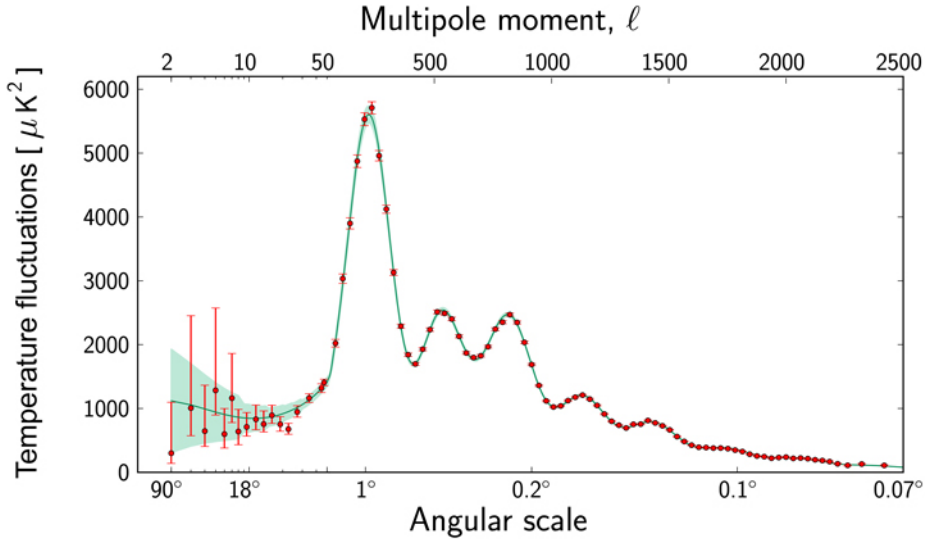
Figure 3: CMB Temperature Anistropy as observed by Planck Satellite from Ref. [6]

.

pressure of the photons coupled to the ionized baryons resists this compression resulting in oscillations. Different scales oscillate at different frequencies so that so some scales reach extrema at the time of recombination inducing maxima and minima in the anisotropies present in the CMB [21]. Measurements of these anisotropies by Planck provide motivation for considering a time and spatially varying α as we expect to see a connection between the decoupling of photons, the atomic formation during recombination and perturbation evolution over time. This happens because change in α would lead cause shift in binding energy of hydrogen atom during the reionization epoch and therefore the redshift. The Thomson scattering cross section is also changed for all particles, since it is proportional to α^2, further elaborated in the next section.

D. Thomson Scattering

Thomson Scattering is the light scattering of free electrons in low energy limit. This becomes important when we study the physics of recombination. As the hot plasma that used to be our universe cools down enough, first hydrogen atoms start forming. However, since these hydrogen atoms form in very high energy state, the electrons emit photons to

get to low energy states by: emitting photon to go from 2p to 1s(rate, $\Gamma \propto \alpha^3$), or 2s to 1s ($\Gamma \propto \alpha^8$) energy levels or and higher-n Rydberg transitions [16]. This process is known as decoupling. The exact time of decoupling is then dependent on the Thomson cross section described as:

$$\sigma_T = \frac{8\pi\alpha^2\hbar^2}{(3m_e^2c^2)}. \tag{30}$$

Thomson scattering also effects the CMB through the surface of last scattering. The CMB radiation we observe today from recombination appears as if it were coming from a spherical shell. It is called the surface of last scattering. Although our universe mostly appear to be homogeneous, we observe matter inhomogeneities in the scale of 10 MPc. During recombination around $t_s \sim H^{-1}$, some scattering still occurs. This causes baryons to experience a drag from the photons. Perturbation analysis shows that the result is damping of baryon fluctuations on scales below the characteristic length the photons propagate. This phenomenon is called silk damping. Theories regarding large scale structure suggest that these inhomogeneities left their imprint in the CMB which we would observe today as temperature anisotropies.

E. Acoustic Oscillations: Peaks in the CMB Power Spectrum

If we closely look at the features of the CMB power spectra, we notice peaks in the oscillation. They are generated from acoustic oscillations in the photon-baryon fluid in cold dark matter gravitational potential wells. As we previously discussed that the early universe was extremely hot and therefore ionized and behaved like plasma. These primordial plasma in the in the early universe caused photon-baryon interaction. Their interactions created an enormous amount of outward pressure against the gravitational force by dark matter that was concentrated at the center. These counter interacting forces created acoustic oscillations. We can actually formalize this to understand how each of the peaks arises in the power spectra. Since we are dealing with fluctuations in a perfect fluid, we can write down our dynamic fluid equations as Fourier mode where we decompose the monopole of the temperature field into:

$$\Theta_{l=0,m=0}(\mathbf{x}) = \int \frac{d^3k}{(2\pi)^3} e^{i\mathbf{k}\cdot\mathbf{x}} \Theta(\mathbf{k}), \tag{31}$$
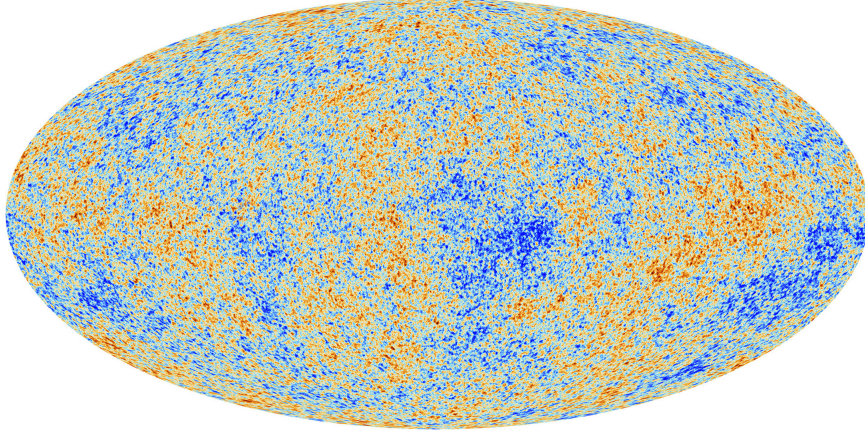
Figure 4: CMB Temperature Map of the universe from Ref. [1]

.

and assume the temperature perturbations obey $\dot{\theta} = -\frac{1}{3}k\nu_\lambda$ which is the continuity equation in Fourier space with ν as fluid velocity and k as the wave number given by $2\pi/\lambda$. In terms of multipoles, ν will be a dipole moment in k direction. Finally, the 1/3rd in this equation comes from the relation $n_\gamma \propto T^3$. Assuming no gravity, and no viscosity, using Euler equation in Fourier space, we obtain:

$$\ddot{\theta} + c_s^2 k^2 \Theta = 0. \tag{32}$$

where $c_s = \sqrt{\dot{p}/\dot{\rho}} = 1/3$ is the sound speed in the fluid. This has solution

$$\Theta = \Theta(0)\cos\left(ks_{\mathrm{rec}}\right) + \frac{\theta(0)}{kc_s}\sin(ks), \tag{33}$$

where s is the distance sound can go within some finite time, also known as the sound horizon. When $ks << 1$, the perturbation directly depends on initial conditions. This is why we can extract information about inflation, large scale structure from CMB power spectra. The oscillations of these Fourier modes can be thought of as terrestrial fluctuations in power spectra. Modes caught at their maxima during recombination are seen as peaks in the power spectra.

So far, we have considered Temperature distribution without gravitational effects. But when we consider initial condition that becomes important. We get an extra term in our solution that shows the tension between pressure gradient from photon baryon interaction and gravitational potential gradient. Thus the compression from gravity and decompression from pressure thus creates sound oscillations. The first peak in the CMB corresponds to

the mode that is caught in its first compression by recombination. The second peak at roughly half the wavelength corresponds to the mode that went through a full cycle of compression and decompression by recombination. On the other hand, for photons to climb out of the gravitational potential well after recombination, they experience a small redshift which shows up in the temperature anisotropy as we see in figure 4.

However, after recombination, photons stop interacting with baryonic matter and we enter matter domination era from radiation domination. During radiation era, radiation drove the acoustic oscillations by making the gravitational force evolve with time [22]. However, matter does not do that. Therefore, the acoustic oscillations starts to diffuse away. This diffusion damping takes place in length scales of $\lambda \leq \lambda_D = \lambda \sqrt{N}$ where $\lambda = \frac{1}{n_e/\sigma_T}$ which is the mean-free path to Thomson scattering and $N = c/(H\lambda)$ is the mean number of scattering events experienced by a CMB photon prior to decoupling. As the background density decreases with time, the potential decreases too. This allows the compressed fluid to leave without dealing with any gravitational potential. The universe at that time, becomes cold dark matter dominated instead of baryon-photon interaction dominated allowing the acoustic peak to rise as matter to radiation ratio decrease. That is the third peak in the CMB power spectra. After that we see the power spectra mostly diffuses away.

Because of these, the sensitivity of CMB to α depend on spatial dynamics of recombination and damping of perturbation.

F. The BSBM and the Runaway Dilaton Model

In Section 2.2, we talked about using scalar field to account for dynamic vacuum energy. The scalar field is also used in high dimensional unification theories to make the extra dimensions small. Since we only observe four dimensions, it is likely that the extra dimensions are small. The scalar field associated with extra dimensions, make sure that the extra dimensions are small and stable [29]. The stability condition is important because most of the times, the scalar field will be coupled to the matter fields. Any time or spatial variations of this field will then be seen as a variation of the interactions' coupling constants.

One of the first attempt for unifying fundamental constant was Kaluza-Klein's 5D theory (see Ref. [23, 25]) for unifying electromagnetism and gravity. Compactification of the fifth dimension, resulted into coupling with a scalar field and matter. Time variation of α was also

analyzed for a self-consistent relations if there are simultaneous variations of the different coupling constants [27]. Other five-dimensional theories, based on Brane-World models, were also used to study variations of the fine structure constant [4, 32, 37]. Relatively recently developed super string theory models also allows variation in the fine structure constant [11].

G. BSBM Model

Without assuming any extra dimensions, Beckenstein formulated a model that allows fine structure constant to vary using a classical description of the electromagnetic field and made a set of assumptions to modify Maxwell equations to take into account the effect of the variation of the charge of electron. In his theory, the scalar field coupled to matter fields which interact electromagnetically. However, he did not take the effect of field on Einstein's equation into account. This was later generalized to include gravitational effects by Sandvik, Barrow and Magueijo.

Beckenstein's formalism for allowing e to change while keeping Planck's constant and c constant and varying α can be done by letting e take on the value of a real scalar field which varies in space and time $e_0 \to e = e_0 \epsilon \left(x^\mu\right)$ where ϵ is dimensionless scalar field similar to ϕ in our previous discussions. e here is the electromagnetic coupling. Then e couples with the Gauge field as A_μ in the Lagrangian. Then under the Gauge transformation $(\phi(x) = e^{i\theta(x)\phi(x)})$, the action is still invariant [35]. For constant ϵ, the Lagrangian of the electromagnetic field is $\mathcal{L}_{cm} = -F^{\mu\nu}F_{\mu\nu}/4$ where $F_{\mu\nu}$ is the Gauge invariant electromagnetic field tensor. The dynamics of the field is controlled by kinetic term $\mathcal{L}_\epsilon = -\frac{1}{2}\omega\left(\epsilon_{,\mu}\epsilon^{,\mu}\right)/\epsilon^2$ as in [3]. In the kinetic term w is hc/l^2 with l being the characteristic length. Beckenstein's theory can be generalized for a cosmological constant by invoking gravitational dependence. Using the transformation $\epsilon \to \phi \equiv \ln \epsilon$, the total action in a cosmological scenario for an accelerating universe can be written as

$$S = \int d^4x \sqrt{-g}\left(\mathcal{L}_g + \mathcal{L}_{\text{mat}} + \mathcal{L}_\phi + \mathcal{L}_{\text{em}}e^{-2\phi}\right). \tag{34}$$

To obtain cosmological equation for the dynamics of the scalar field, the action can be varied with respect to the metric to obtain Einstein's equation:

$$G_{\mu\nu} = 8\pi G\left(T_{\mu\nu}^{\text{mat}} + T_{\mu\nu}^\phi + T_{\mu\nu}^{em}e^{-2\phi}\right), \tag{35}$$

and varying with respect to ϕ gives dynamic equation of motion for the scalar field as:

$$\Box\phi = \frac{2}{\omega}e^{-2\phi}\mathcal{L}_{\text{em}}. \tag{36}$$

$\mathcal{L}$ vanishes for a sea of pure radiation. Then $\mathcal{L}_{\text{em}} = E^2 - B^2 = 0$. This will suggest insignificant changes in e during radiation epoch which however is not the case for matter epoch. The contribution of matter to the right hand side of the equation can be written using the parametrization $\zeta = \mathcal{L}_{\text{em}}/\rho$.

Assuming a spatially flat, homogeneous universe (assumptions we used for FRW metric), we can write down Friedmann equation for this model:

$$\left(\frac{\dot{a}}{a}\right)^2 = \frac{8\pi}{3}\left(\rho_m\left(1 + \zeta_m e^{-2\phi}\right) + \rho_r e^{-2\phi} + \rho_\phi + \rho_\Lambda\right). \tag{37}$$

Using Eq. (37), we can also write down conservation equations for the non-interacting radiation (using $\tilde{\rho}_r \equiv \rho_r e^{-2\phi} \propto a^{-4}$) and matter density

$$\begin{aligned}
\rho_m + 3H\rho_m &= 0 \\
\dot{\tilde{\rho}}_r + 4H\tilde{\rho}_r &= 0
\end{aligned} \tag{38}$$

This gives us a Friedmann universe consistent with time variation of α. The variation of ϕ is almost constant during radiation epoch because of the Lagrangian but during matter epoch α increase slightly towards lower redshifts and leans towards being constant values as dark energy takes over. This reduction in α variations is strongly constrained by observations [9]. We will look at constraints of coupling on this model based on the work in [3] and Planck CMB data for time variation in α.

H. Runaway Dilaton Model

The other theoretical model that we consider for this work is the Runaway Dilaton model. It is a string theory inspired model that has low energy and the extra dimensions are coupled with a massless scalar field called Dilaton. If the dilaton has an order unity coupling to the dark sector, the runaway of the dilaton towards strong coupling can give us dynamical dark energy, violations of the Equivalence Principle and variations of α. For smaller couplings, the model is equivalent to ΛCDM.The potential for strong and weak coupling can be shown similar to Fig 5. A standard solution for this stabilizes the dilaton in the weak coupling
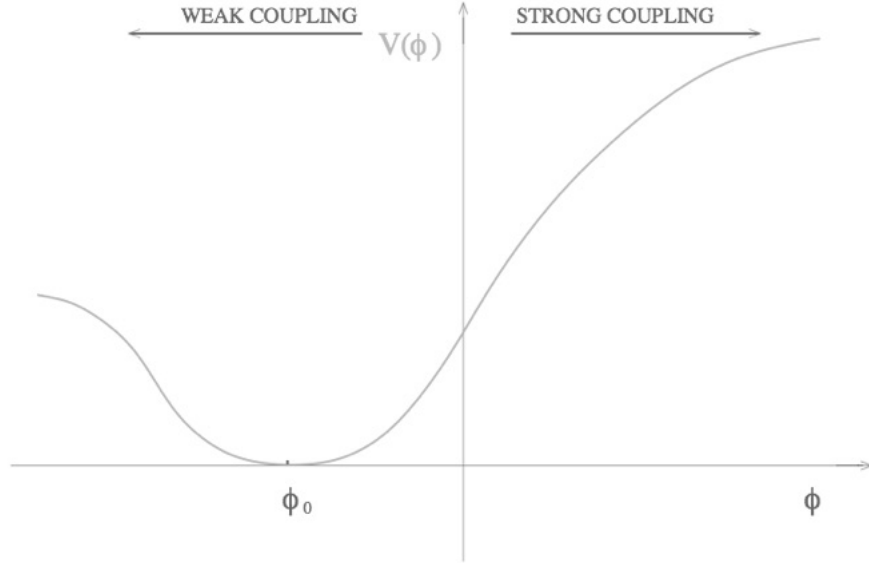
Figure 5: Scalar field potential evolution for strong and weak coupling. Image credit: Perimeter Institute.

region and gives the dilaton a mass and shortens its interaction range. The strong coupling can be corrected by trivializing the coupling at a constant value at infinity [28].

$$B_i(\phi) = c_i + \mathcal{O}\left(e^{-\phi}\right) \tag{39}$$

The Lagrangian for the Runaway dilaton is defined as (for further discussion see [7, 11]):

$$\mathcal{L} = \frac{R}{16\pi G} - \frac{1}{8\pi G}(\nabla\phi)^2 - \frac{1}{4}B_F(\phi)F^2 + \ldots, \tag{40}$$

where R is the Ricci scalar and B_F is the gauge coupling function. One can show the Friedmann equation for this model is [28].

$$3H^2 = 8\pi G \sum_i \rho_i + H^2\phi'^2. \tag{41}$$

The sum over ρ is over all the components of the universe and the dilaton potential. The kinetic energy of the scalar field is included in the last term. The derivative is with respect to $p = \ln a +$ const. The total pressure and density for this system is then

$$\rho_\phi = \rho_k + \rho_v = \frac{(H\phi')^2}{8\pi G} + V(\phi) \tag{42}$$

$$p_\phi = p_k + p_v = \frac{(H\phi')^2}{8\pi G} - V(\phi). \tag{43}$$

This is similar to the quintessence case as we described in BSBM model. In low energy level, both of the scalar field behave similarly. Using the Lagrangian and the described transformation using logarithm of the scaling factor, the equation of motion can also be written as below[11].

$$\frac{2}{3 - \phi'^2}\phi'' + \left(1 - \frac{P}{\rho}\right)\phi' = -\sum_A \alpha_A(\phi)\left(\frac{\rho_A - 3P_A}{\rho}\right) \tag{44}$$

The sum of ρ and P in this equation the total energy density and pressure respectively, both obtained as sums over the various components that fills the universe except the kinetic energy density and pressure of the scalar field as shown above. The $\alpha_A(\phi)$ term on the right hand side is a dimensionless quantity that measures coupling of the scalar field of different particle types defined as:

$$\alpha_A(\phi) \equiv \frac{\partial \ln m_A(\phi)}{\partial \phi}. \tag{45}$$

For this work, we consider both the electromagnetic and matter coupling separately and explicitly add dark energy to the density equations. The dynamic equation used for this work with necessary couplings is explicitly explained and demonstrated in Section IV.

III.   UNDERSTANDING THE NUMERICAL METHODS

For this work, we constrain couplings and free parameters in the larger theoretical models described above to find cosmological models that are consistent with α variation. Instead of directly using the models to reconstruct CMB power spectra, we build on the work of Ref. [17] where they calculated principal components which represent the directions of the CMB data that explain a maximal amount of variance (further discussion on the numerical method below). Using their work, we see how much different PCs each models mix and produce and minimize that difference.

A.   Principal Component Analysis

Principal component analysis is a way of reducing dimensional analysis calculation while preserving most of the information. In other words, we compose a list of different characteristics of some objects in our case fundamental constants. And since many of them will
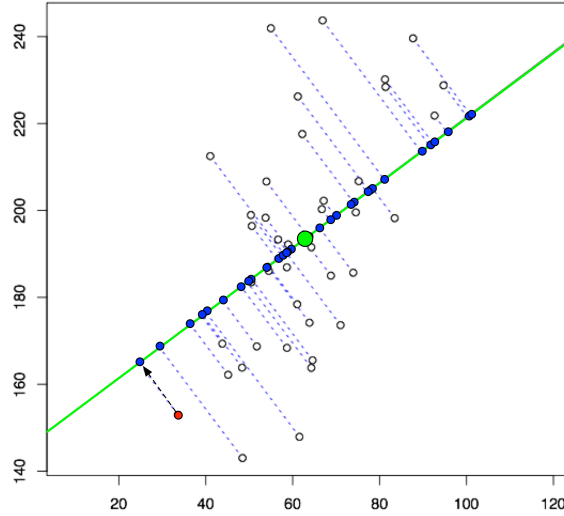
Figure 6: Finding best fit line of a data set using Principal Component Analysis, adopted from Ref. [31].

measure related properties , we are able to summarize each variation with fewer characteristics. PCA looks for properties that show as much variation as possible and are able to reconstruct the original characteristics. When a few properties are correlated, we can reconstruct a new property by projected all the points in the plain on some line that is given by some linear combination $\lambda_1 x + \lambda_2 y + \lambda_3 z$. PCA finds the best fit value of all the possible linear combination by keeping the variance highest and error lowest. In figure 3.1, as we can see, the spread of the white dots is the average squared distance from the center of the data to each white dot known, also known as variance in statistical terms. On the other hand, the total reconstruction error is measured as the average squared length of the corresponding dotted lines. But as the angle between dotted lines and the green line is always 90, the sum of these two quantities is equal to the average squared distance between the center of the data and each white dot. This average distance does not depend on the orientation of the green line, so the higher the variance the lower the error as their sum is constant. Now, the way we achieve this is by taking a co variance matrix which is a $n \times n$ symmetric matrix that has as entries the covariances of all possible pairs of the initial variables. For a three

dimensional case it can be written as

$$
\begin{bmatrix}
\text{Cov}(x,x) & \text{Cov}(x,y) & \text{Cov}(x,z) \\
\text{Cov}(y,x) & \text{Cov}(y,y) & \text{Cov}(y,z) \\
\text{Cov}(z,x) & \text{Cov}(z,y) & \text{Cov}(z,z)
\end{bmatrix},
\tag{46}
$$

where the covariance of with itself is simply the variance. Now this matrix can be diagonalized by simply transforming it with orthogonal basis given by it's eigenvalue which transforms the above matrix to

$$
\begin{bmatrix}
\text{Cov}(x,x) & 0 & 0 \\
0 & \text{Cov}(y,y) & 0 \\
0 & 0 & \text{Cov}(z,z)
\end{bmatrix}.
\tag{47}
$$

What this means is that there is no correlation between any two points. Therefore, the maximum variance is achieved when we take the projection on the first coordinate axis. It follows that the direction of the first principal component is given by the first eigenvector of the covariance matrix.

For our mentioned model parameter variations, PCA will allow us to forecast uncertainties with which we can determine our model parameters. To achieve this, we use something called the fisher matrix which will let us calculate the covariance matrix associated with maximum-likelihood estimates. Assuming our model is dependent on a set of parameters $\Gamma = \gamma_1, \gamma_2, \ldots$. However, since we do not know true values for γ_n, each of the parameter "guess" will have some error, σ. So, we use a method called Best Unbiased Estimator. Now since for each value of our parameters, there will be some uncertainty, we can write down a likelihood function $L(x, \Gamma)$ where x is probability of making any observation. In order to extract information from a set of existing observations x_0, the maximum likelihood estimator is used that gives parameter estimate that maximizes the likelihood function for $x = x_0$ as for a large data set, the maximum likelihood estimator approaches a Best Unbiased Estimator.

If the parameter estimate is an unbiased function, then $\sigma_i \geq F_{ij}{}^{-1}$ where F is the Fisher Matrix (Using Kramer-Rao Inequality) [18]. The entries of the Fisher Matrix is defined as:

$$
F_{ij} = \left\langle \frac{\partial^2 \mathcal{L}}{\partial \theta_i \partial \theta_j} \right\rangle
$$

For our purpose, we can write the likelihood function as $\mathcal{L}(\vec{p} \mid \mathbf{d}, M)$ where M is our model, d is Planck data and p is parameter for such a model. The Fisher matrix then for CMB can

be written as

$$F_{ij} = \left(\frac{\partial^2 \ln \mathcal{L}}{\partial p_i^2} \right) = \sum_{l=0}^{t_{\max}} \frac{\partial \vec{C}_l}{\partial p_i} \cdot \mathbf{\Sigma}_t^{-1} \cdot \frac{\partial \vec{C}_l}{\partial p_j}, \tag{48}$$

where the CMB power spectra vector is given by, $\vec{C}_\ell = \left(C_t^{TT}, C_t^{EE}, C_l^{TE} \right)$ Here the TT, TE, EE power spectra are taken into account because CMB light coming from a given direction in space has both an intensity and a polarization. Planck satellite can measure both and allows us to look at polarization-polarization(EE), intensity-polarization(TE), intensity-intensity(TT). Then the covariance matrix for a given multipole ℓ is,

$$\Sigma_\ell = \frac{2}{2\ell + 1} \begin{bmatrix} C^{TT^2} & C^{TE^2} & C^{TT}C^{TE} \\ C^{TE^2} & C^{\mathrm{EE}^2} & C^{\mathrm{TE}}C^{\mathrm{EE}} \\ C^{\mathrm{TT}}C^{\mathrm{TE}} & C^{\mathrm{TE}}C^{\mathrm{EE}} & \frac{1}{2}\left(C^{\mathrm{TE}^2} + C^{\mathrm{TT}}C^{\mathrm{EE}} \right) \end{bmatrix}_\ell. \tag{49}$$

We assume there to be no cross-multipole correlations which allows us to use the defined CMB fisher matrix entries.

Ref. [17] used this formalism to generate principle components for α variation. In 3.3, instead of ρ, they used α in the fisher matrix. Then they generated principal components from the Fisher matrix for α variation by diagonalising and decomposed the fisher matrix into its eigenbasis such that,

$$F_{ij} = S_{im}.F_{mn}.S_{nj}, \tag{50}$$

where S_{im} is the matrix of eigenvectors of the Fisher matrix and F_{mn} is a diagonalised matrix of the eigenvalues. These eigenvectors are recast as eigenfunctions using the basis functions generated by a complete set of basis functions, $\phi_i(z)$, over the redshift space $z_i \in (300, 2000)$. This can be formally written as:

$$E_m(z) = \sum_{i=1}^{N} S_{im}\phi_i(z). \tag{51}$$

Here E_m is the principal component. And as discussed, E_1 will contain most information, E_2 after that and then E_3. CMB angular power spectra for a fine structure constant model is shown in fig 7. The eigenmodes propagate through the Thomson optical path which is is a measure of opaqueness along the path of light due to Thomson scattering, and then onto the CMB.
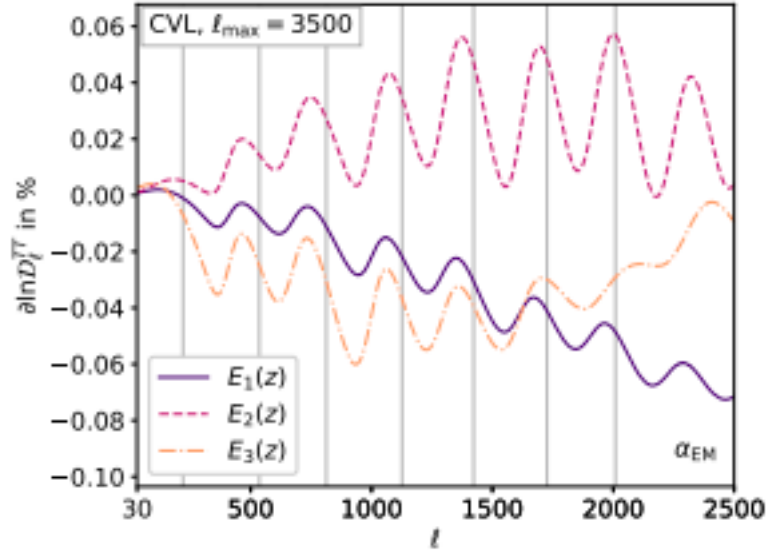
Figure 7: Fine structure constant PCA eigenmodes for Cosmic Variance experiment with the grey-lines as peaks of the Planck fiducial power spectra as seen in Ref [17]

B.   Monte Carlo Markov Chain

To understand how Monte Carlo Markov Chain is used for this work, we'll be revisiting a few statistical results. Monte Carlo simulation is a numerical technique of sampling random distribution from data without knowing the true underlying distribution to draw inference about the population. For Monte Carlo simulation, we need to understand dependent probability well.

To dive into this, we can discuss the can discuss seemingly simple yet elegant Monte Hall problem. The problem is simple: Imagine a gaming show where you have to guess what is behind a closed door. For simplicity imagine 3 doors and you are told there's a car behind one of them. Now, if you guess the right door you win the money. To begin with, the probability of you choosing the right door is 1/3. Now, the host of the show opens one of the doors and shows you that it is empty. He also gives you a chance to change your answer. The question is should you stick to your first choice or change your answer. Which door should you choose to have better odds of winning?

It is often intuitive to think now that one door is eliminated the probability of you choosing the right door is 0.5. However, this is not the case. The probability of the door you chose first being right is still 1/3. However, if you switch the odds of you winning is

2/3. Why is that? Because, the odds of the car being behind the two doors that you did not choose was 2/3. Once one of the doors is opened and because since the host knows it is empty, the probability is concentrated on the remaining door. We can now formalize this idea.

For two events A and B, we will denote P(A) as probability of A, P(B) probability of B, probability of B given A as $P(A|B)$. We will consider that event A and B are dependent events. Then P(A and B) = P(A) $P(A|B)$. Since P(A and B) is the same as P(B and A), we get:

$$P(A|B) = \frac{P(A)P(B|A)}{P(B)}. \tag{52}$$

This is Bayes's theorem. Now, for our work we can imagine event A as Hypothesis and B as Data. Then, we rewrite Bayes's theorem transform in this new notation as:

$$P(H|D) = \frac{P(H)P(D|H)}{P(D)}, \tag{53}$$

where P(H) is the probability of the hypothesis before we using the observed data, called the prior; $P(H|D)$ is the probability of the hypothesis after we use observational data, called the posterior, $P(D|H)$ is the probability of the data under the hypothesis, called the likelihood and P(D) is the probability of the data under any hypothesis. P(D) is typically just a normalizing constant (If we plug in probability and likelihood for the three possibilities in Monte Hall problem we can actually check see the posterior increasing for switching doors).

For our work, we are interested in the distribution of the parameters. We do this by generating random numbers from a normal distribution which we can think of as a proposal distribution. If we draw a density plot (histogram) of the randomly generated samples, for a large enough sampling, the density curve will have a similar shape to the proposal distribution. However, in this case we are not assuming the proposal distribution does not change for one iteration to the next. However, as we have seen in Monte Hall problem that can lead us to incorrect estimates. So, for Monte Carlo simulation, we make sure that each point in the density plot is dependent on the previous one. Each value this time is drawn from a normal distribution which has mean equal to previous value of the generated sample. The path of this is called a random walk. In this case, however, the density plot is not the same distribution as the one the samples were drawn from. However, for a Monte Carlo simulation, we do not accept all the randomly generated samples since that will not give us a good estimate for our data. So, instead what we do is, we calculate posterior using for

some randomly generated value. We can do so by multiplying the prior distribution by the likelihood function. Then if the ratio of the probability of the new value and the previous one is greater than 1, we always accept the new sample. However, we do not discard the rest of the samples. Rather, we use the ones with ratio less than ones as acceptance probability. We then draw a uniform random distribution. If the random number is less than acceptance probability, we reject it.

Although this is the idea behind the most simple MCMC algorithm, The Metropolis-Hastings, for our work we use a slightly more efficient version of this. The MCMC in this method is done by advancing an ensemble of K walkers based on the state of the ensemble where the proposal distribution for one walker k is based on the current positions of the K-1 walkers in the complementary set of the parameter space. To update position of the walker at some position X_k, a walker X_j is randomly chosen from the remaining walkers and a new position is proposed as seen in [13]:

$$X_k(t) \to Y = X_j + Z\left[X_k(t) - X_j\right], \tag{54}$$

where Z is a random variable drawn from a distribution g that satisfies $g\left(z^{-1}\right) = zg(z)$ and

$$g(z) \propto \begin{cases} \frac{1}{\sqrt{z}} & \text{if } z \in \left[\frac{1}{a}, a\right] \\ 0 & \text{otherwise} \end{cases} \tag{55}$$

The probability of accepting the proposal is:

$$q = \min\left(1, Z^{N-1} \frac{p(Y)}{p\left(X_k(t)\right)}\right). \tag{56}$$

However, since our proposal distribution is symmetric in Eq. (54), evolving walkers in parallel can disrupt the balance. So, we split the full ensemble into two subsets and simultaneously update all the walkers in one subset based only on the positions of the walkers in the other subset using Eq. (54), (55) and, (56). Then we use the updated subset to update position of the walkers of in the subset the update was based on.

The generic parallelization make this algorithm extremely accurate. We use the emcee package for this work that implements this algorithm for constraining our parameters.

IV.   CALCULATIONS AND RESULTS

As stated in previous sections: we chose two models to explore α variation in: BSBM and runaway Dilaton Model. We use the general dynamic equations discussed in Important
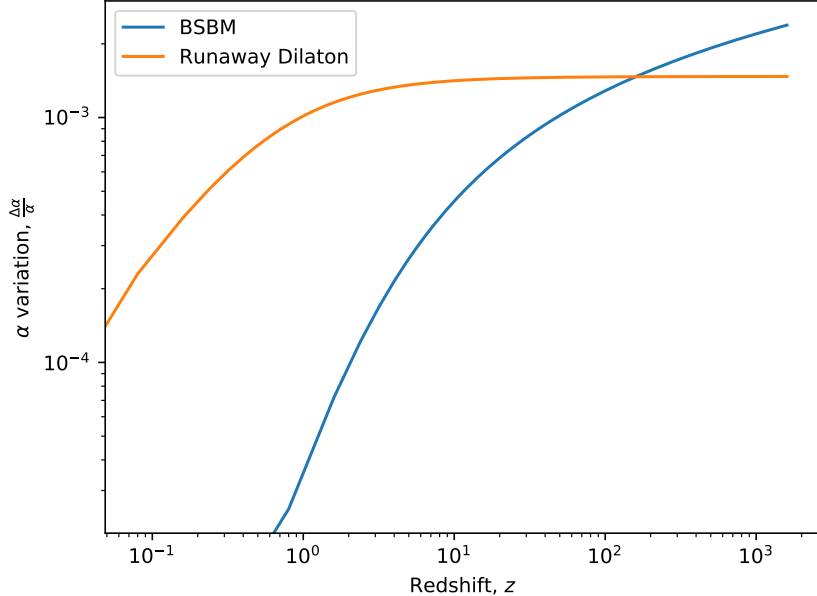
Figure 8: Time variation of α as a function of redshift for BSBM and Runaway Dilaton governed universe

physical background section with some parametrization discussed below. Since the QSO data we are using for this work is given as function of redshift, we evolve α variation in these two models as seen in fig 8.

A.   BSBM

For our work, we assume a spatially flat, homogeneous, and isotropic universe that abides by the Friedmann equation with expansion scale factor a(t). From section 2.6, we can write down the general equation for BSBM as [the $\Box$ is the same operator described in Eq. (16)]:

$$\Box\phi = -\frac{2}{\omega}e^{-2\phi}\zeta_m\rho_m. \tag{57}$$

The scalar field ϕ plays a similar role to the dilaton in the low-energy limit with the important difference that it couples only to electromagnetic energy. The $\zeta_m\rho_m$ term comes from Lagrangian of the field which is simply $E^2 - B^2$. During matter domination, change in e can occur. ζ_m comes from the parametrized ratio of the Lagrangian and energy density. Therefore the value of ζ_m depends protons, neutrino mass, as well as contribution from current

of quarks as the Lagrangian is $E^2/2$. However, it also has to account for the non-baryonic fraction of matter. Thus the value of ζ_m can span a wide range of values depending on the nature of the dark matter (e.g. for superconducting cosmic strings $\zeta_m = -1$ whereas for neutrinos $\zeta_m \ll 1$). The value for ζ_m is between [-1,1]. Through our work we constrain this parameter using both QSO and CMB data to see if that allows α variation with time. Another parameter we let vary is the mass that comes from the potential when we set it to $m^2\phi^2$.

For BSBM model, we use everything in Planck unit with $h = c = 1$ and $M = M_{\rm pl}$. We are also considering a ΛCDM universe where the cosmological constant Ω_Λ is 0.6825, matter density $\Omega_m = 0.3175$. For radiation density, we consider both present-day photon density and the neutrino density. The neutrino density is related to the photon density by

$$\rho_v = 3.046\frac{7}{8}\left(\frac{4}{11}\right)^{4/3}\rho_\gamma, \tag{58}$$

where ρ_ν and ρ_γ is neutrino and photon density respectively. The photon density can be written as:

$$\rho_\gamma c^2 = \int_0^\infty h v n(v)\mathrm{d}v = a_B T_0^4, \tag{59}$$

where $a_B = \frac{8\pi^5 k_B^4}{15 h^3 c^3}$ with k_B as Boltzmann's constant. By plugging in $T_0 = 2.725$ as observed by Plank, we get radiation density

$$\Omega_r = \left(\Omega_\gamma h^2 + \Omega_v h^2\right) h^2 = 9.235 \times 10^{-5}. \tag{60}$$

Now, Eq. (57) shows the scalar field as a function of time. However, our motivation for this work is drawn from the QSO observation which provides evidence for possible α variation shown in fig 9. Since the data we are using provides alpha variation with redshift, we rewrite our dynamic equation as a function of redshift assuming the redshift is zero at present day and we go backwards in time. So, we write the dynamic equation with the following conversions:

$$H = H_0(\Omega_m(1+z)^3 + \Omega_r(1+z)^4 + \Omega_\Lambda) \;,\; \frac{\dot{a}}{a} = H \;,\; a = \frac{1}{1+z}. \tag{61}$$

Using these conversations, for the right hand side, we also make some adjustments as we change everything to Planck unit. We multiply ω in Eq. (57) with a dimensionless quantity
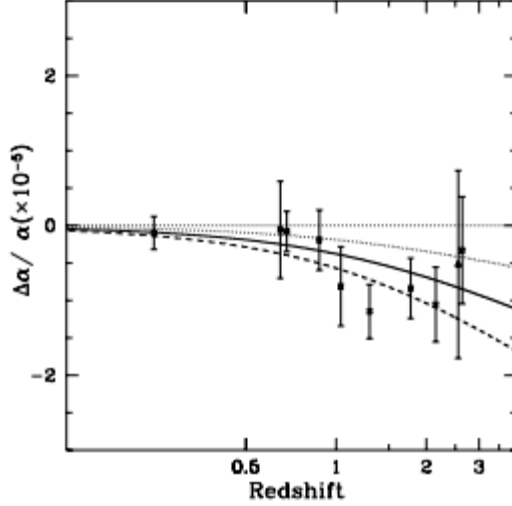
Figure 9: Variation of α using Quasar Data with plausible theoretical bestfit lines as seen in Ref. [35]

$\tilde{\omega}$. Then, $\omega = \omega_u \tilde{\omega}$ then $\omega = \left(\frac{\hbar c}{l_p}\right)^2 \tilde{\omega}$. and $\rho_m = \frac{3\Omega_m H_0^2 a^{-3}}{8\pi G}$. Here $\zeta_m = \frac{\mathcal{L}_{em}}{\rho}$, then right hand side of the equation becomes, $\frac{2\zeta_m}{\tilde{\omega}} \frac{l_p^2}{(hc)^2} \frac{3\Omega_m H_0^2 a^{-3}}{8\pi G} e^{-2\phi}$. Here $\frac{1}{8\pi G}$ is M_{pl}^2 and $\left(\frac{l_p}{\hbar c}\right)^2$ has unit length and unit of $\frac{1}{M_{pl}^2}$. Then the right hand side becomes $\frac{6\zeta_m}{w}\Omega_m H_0^2(1+z)^3 e^{-2\phi}$. Combining Eq. (57), (61) we get the dynamic equation for the scalar field is:

$$\frac{d^2\phi}{dz^2} - \frac{d\phi}{dz}\left(\frac{2}{(1+z)} - \frac{(3\Omega_m(1+z) + 4\Omega_r)}{2(\Omega_m(1+z)^3 + \Omega_r(1+z)^4 + \Omega_\Lambda)(1+z)^3}\right)$$
$$+ \frac{m^2\phi}{(1+z)^2(\Omega_m(1+z)^3 + \Omega_r(1+z)^4 + \Omega_\Lambda)}$$
$$= -\frac{6\zeta}{\omega}\frac{\Omega_m(1+z)}{\sqrt{\Omega_m(1+z)^3 + \Omega_r(1+z)^4 + \Omega_\Lambda}}e^{-2\phi}. \quad (62)$$

We can get a an estimate for the QSO bestfit for ζ from Ref. [35] at redshift 3 for 0 mass. ζ_m is predicted to be in the order of 10^{-4} for the above shown theoretical models to be consistent with QSO observed data points and error bars. However, as we let the mass vary we can look at the behavior of the scalar field at redshift 3 and see if that affects our prediction of ζ_m/ω values.

We plot at the behavior of the scalar field in fig 10(a) by numerically solving Eq. (62) for a wide range of values of ζ_m/ω. We also plot the scalar field for Ref. [35]'s bestfit of ζ/ω in black on the same plot. This is fairly simple to do since the scalar field and α variation are related to each other by $\alpha = \exp(2\phi)e_0^2/hc$ (shown earlier). We can then Taylor expand to get $\frac{\Delta\alpha}{\alpha}$ is 2ϕ. Now, we let the scalar field evolve to higher redshifts(earlier times) to
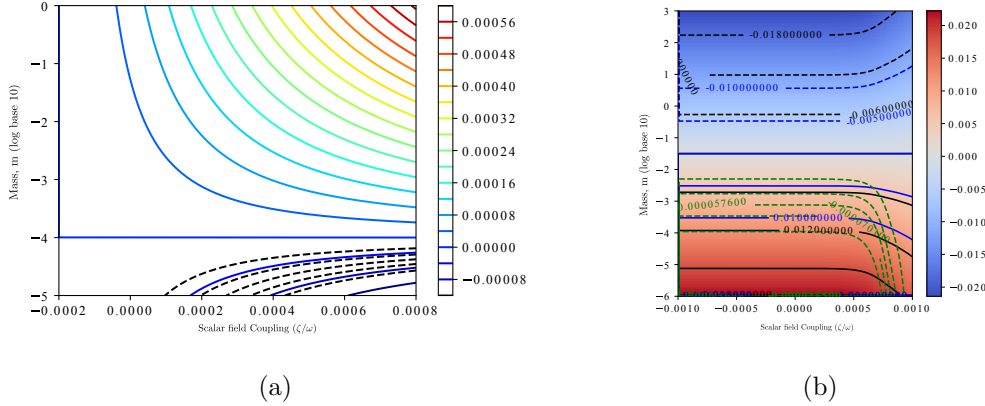
Figure 10: (a) Scalar field at redshift 3 fitted with QSO data(Black dotted lines) while varying mass and coupling ; (b) Scalar field at redshift 1000 fitted with QSO data (Green dotted lines), CMB constraints with Planck error bars(black lines) and CMB constrains with 0 α variation with Planck error bar (blue lines) while varying mass and coupling

predict what happens during recombination. This also allows us to see if the α variation is consistent across time. We do so by numerically evaluating the scalar field at redshift 1000 again allowing ζ/ω and m to vary a wide range of values. We then show scalar field contours for ζ/ω bestfits at QSO, for zero α variation with Planck errorbar during recombination, α variation prediction from Planck data up to 2σ in fig 10(b).

This analysis inspired us to further analyze α variation at CMB since we see promising signature of free parameter variation being consistent during both redshift 3 and 1000. We use principle component analysis to do so.

Ref. [18] gives us PCA Eigenmodes for fundamental constant variation. Their work also paves a way for adding linear change to parameter variations. The generic variation in some fundamental constants C as a function of eigenmodes constrained in the analytic method is defined by:

$$\rho_i = \int \frac{\Delta C}{C}(z) \cdot E_i(z)dz. \tag{63}$$

The assumption for calculating variation this is that we are in some perturbative regime where the relative change in the constant is proportional to the relative change in the model amplitude. Since we assume linearity, we can calculate rho_i as we change parameters which gives us projections of different models. Using PCA Eigenmodes as data, we can write down
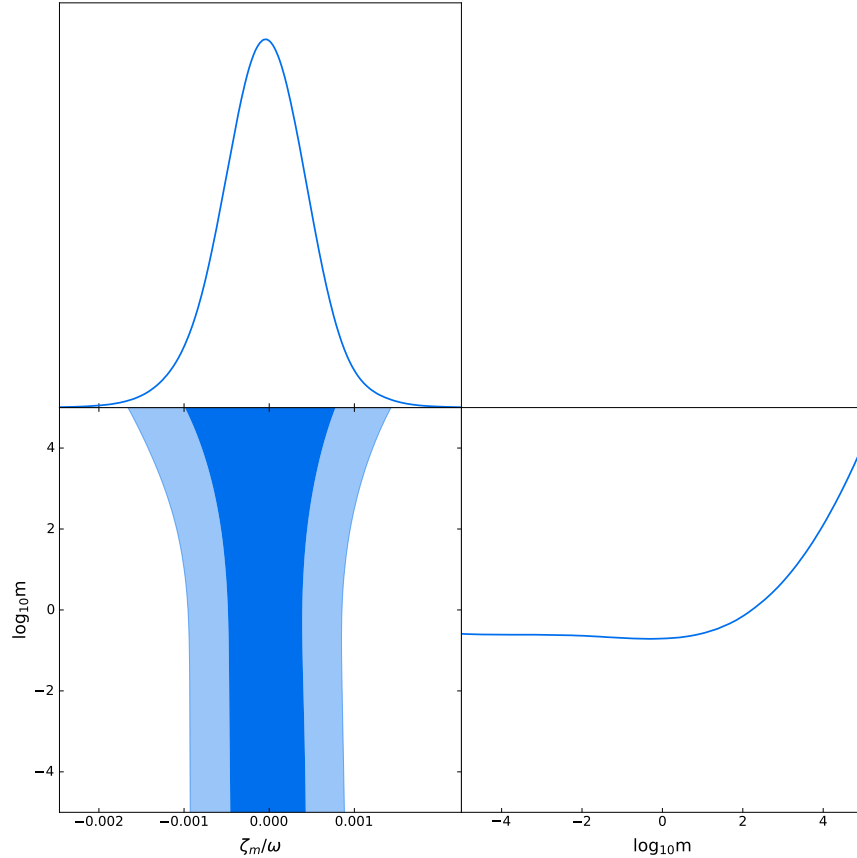
Figure 11: 2σ contours for BSBM coupling and logarithm of mass during recombination from Planck 2018 data using Monte Carlo simulation

χ^2 values for our models as:

$$\chi^2 = (\text{Model}_i - \alpha \ \text{CVL Mode}^1{}_i)^T \Sigma_{ij} (\text{Model}_i - \alpha \ \text{CVL Mode}_i). \qquad (64)$$

Since the likelihood for this is just $e^{-\chi^2/2}$, minimizing 3.5 gives us the actual bestfit values. Although, we can do that directly using the information we have now, this method only allows us to vary one parameter at a time. So, we use MCMC since it allows sampling from a probability distribution as described in Understanding the Numerical Methods Section. We use a python package named emcee.

The way emcee works is that the algorithm simultaneously evolves an ensemble of K walkers $S = X_k$ where distribution for one walker k is based on the current positions of the $K - 1$ walkers in the complementary ensemble. This process is continued and repeated for each walker in the ensembled series till the MCMC chain is repeated [13].

---

[1] Ref [17] generated eigenmodes for a cosmic-variance-limited (CVL) experimental setup and investigated
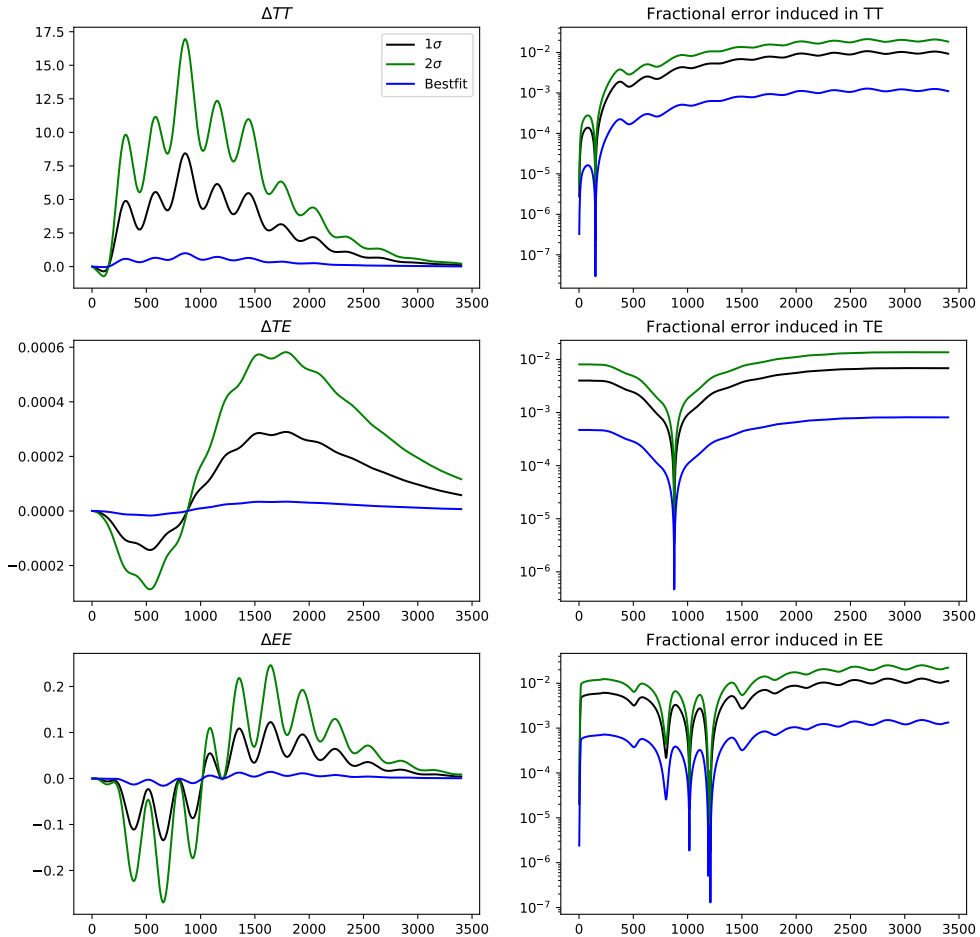
Figure 12: Change in C_ℓ due to excitation in principle components for change in coupling and mass at bestfit, one σ and two σ level.

For our work, we use this algorithm for minimizing $-\chi^2/2$ value as we let both of our parameters vary. We calculate ρ using Eq. (63) and use Ref. [18]'s PCA eigenmodes as data points for "observations" at recombination. The resulting constraints including and upto 2σ is shown in figure 10. As we can see, when the field becomes extremely massive, mass becomes unconstrained and for all ζ/ω values we get a good fit that is consistent with Planck.

Any Principle Component is a change in $\alpha(z)$ that induces a change in C_ℓ that is de-

the structure and propagation from these variations in α_{EM} to the CMB anisotropies.

tectable at 1σ if $\alpha(z) = \alpha_0(1 + \sigma_i E_i(z))$. We use Ref. [18]'s ΔC_ℓ values for the three PC's and adopt them for our model by:

$$\Delta C_\ell^{\text{BSBM}} = \sum_{i=1}^{N_{\text{pc}}} \rho_j \Delta C_\ell^j. \tag{65}$$

We show change in C_ℓ at one σ level for our parameter constrain from MCMC chains in Fig 12.

B.   Runaway Dilaton

From our previous discussion on Runaway Dilaton, we have the governing equation for a dilaton governed universe as:

$$\frac{2}{3 - \phi'^2}\phi'' + \left(1 - \frac{P}{\rho}\right)\phi' = -\sum_A \alpha_A(\phi)\left(\frac{\rho_A - 3P_A}{\rho}\right). \tag{66}$$

Here α_A determines the effect of cosmological matter on the evolution of the scalar field [8, 10]. During radiation domination, $\rho_A - 3P_A = 0$ then the driving force vanishes as the right hand side goes to zero and the scalar field is not driven to approach some value towards infinity. Then the approximate value of the scalar field is $\phi = \phi_{end}$. However, this is not the case for matter domination era. For non relativistic matter, the right hand side of the equation is non-zero. In the slow roll approximation, shown in Important Physical Background Section, equation-of-state parameter becomes negligible and we are left with the dark matter coupling to the field

$$\phi_m\prime = \alpha_m(\phi). \tag{67}$$

Note, this α is not the same α we are concerned with throughout this work. From Ref. [11], we have,

$$m_m(\phi) \simeq m_m(+\infty)\left(1 + b_m e^{-c\phi}\right). \tag{68}$$

Then, using Eq. (45), we can write down the matter coupling to the scalar field as $\alpha_m = -\frac{b_m c e^{-c\phi}}{1 + b_m e^{-c\phi}}$. Dark matter couples to the scalar field in the dilaton scenario differently then ordinary matter. Although the density of dark matter is much larger, we still account for baryonic matter on our work to be consistent. Now, going back to our discussion on dilaton coupling, in the string frame, the gauge coupling of the field is linked to the string mass using

Eq. (39). Then we can write down the gauge coupling dependence explicitly as $g_F^2 = B_F(\phi)$. One can show that approximately the the scalar field coupling to hadronic matter can be written as below using the Einstein-frame confinement scale dependence on scalar field:

$$\alpha_{\text{had}}(\phi) \simeq \left[\ln\left(\frac{\widetilde{M}_s}{\Lambda_{\text{QCD}}} \right) + \frac{1}{2} \right] \frac{\partial \ln B_F^{-1}(\phi)}{\partial \phi}. \tag{69}$$

The factor in the right hand-side to a good approximation is 40. Using Eq. (39), the parametrized field coupling gives us:

$$B_F^{-1}(\phi) = B_F^{-1}(+\infty) \left[1 - b_F e^{-c\phi} \right]. \tag{70}$$

Again, using Eq. (45), we can write down the coupling as :

$$\alpha_{had} = 40 \left(\frac{b_F c e^{-c\phi}}{1 - b_{\text{F}} e^{-c\phi}} \right). \tag{71}$$

Since we will be using Planck and QSO data again to constrain couplings in this model, we write down the equation of motion, as a function of redshift. Using the dark matter and baryonic matter dependence, our governing equation of motion is:

$$\frac{4(1+z)^3 \phi\prime}{3 - (1+z)^2 \phi\prime^2} + \frac{2(1+z)^4 \phi\prime\prime}{3 - (1+z)^2 \phi\prime^2} - \left(1 + \frac{\Omega_\Lambda}{\Omega_m(1+z)^3 + \Omega_\Lambda} \right) (1+z)^2 \frac{d\phi}{dz}$$
$$= \frac{b_m c e^{-c\phi}}{1 + b_m e^{-c\phi}} \left(\frac{\rho_{dm}}{\rho} \right) + 40 \left(\frac{b_F c e^{-c\phi}}{1 - b_F e^{-c\phi}} \right) \left(\frac{\rho_{\text{had}}}{\rho} \right). \tag{72}$$

A possible variation of α gives the most constraint on the coupling limit as because of our previous assumptions, $e^2 \propto B_F^{-1}(\phi)$. Then $e^2(\phi) = e(+\infty)[1 - bFe^{-c\phi}]$. Since α is simply $\frac{e^2}{\hbar c}$, we can write down the relation between α variation and the scalar field as below:

$$\frac{\Delta\alpha}{\alpha} = b_F \frac{\left(e^{-c\phi_0} - e^{-c\phi} \right)}{(1 - b_F e^{-c\phi_0})}. \tag{73}$$

For simplicity, we set c=1 and attempt to constrain the gauge coupling b_F, matter coupling b_m and the initial condition $\phi\prime$. Similar to what we did for BSBM, we run Markov chain simulation to draw histograms and find best fit that minimizes χ^2 for α PCs. For this model, we don't have constraints on parameters from previous literature either for our induced general model so, we also run the simulation at redshift 3 and constrain couplings with Quasar data.

The red curves shows best fit for coupling that are consistent with CMB, and blue curves shows best fit for coupling that are consistent with QSO. We see overlap between the two
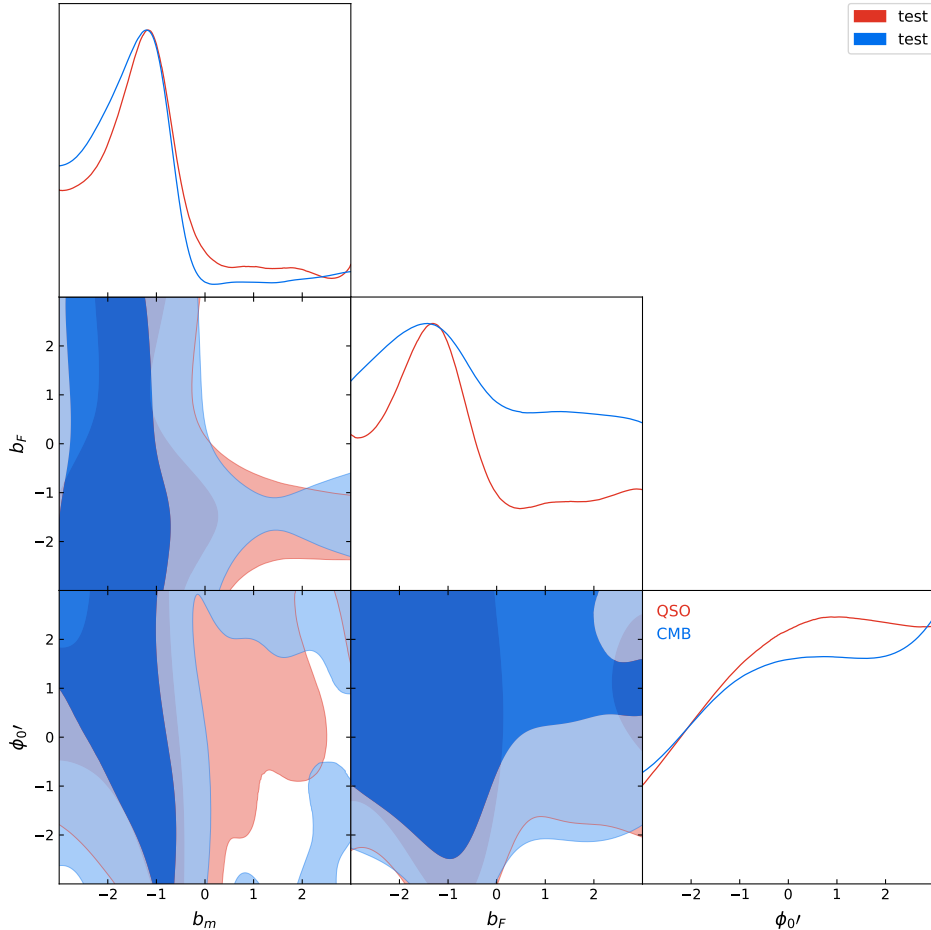
Figure 13: Constraining dilaton couplings using CMB(in blue) and QSO(in red) data

.

regions. Although there is a big degeneracy, the coupling bestfit has overlaps within 1 sigma contours (here 1 σ is the darker blue/red curves). The consistency across both models for alpha variation is highly reassuring. As a next step for this work, we plan to draw residual plots using couplings and free parameter values that are marginally between 1σ and 2σ contours. The idea is to draw the Eigenmode projections using Eq. (63) and comparing with PCs to see how much variation we can expect.

V. CONCLUSION

In this work, we devised a numerical tool to test fine structure constant variation by constraining scalar field couplings and free parameters using Quasar and Cosmic Microwave Background Radiation data. We can also test other theories for α variation using this

method. We have seen evidence for time variation of α across redshift 3 and 1100(approximately).

For future direction of this work, instead of using average value of quasar at Redshift 3, we can explicitly use quasar data points and make more accurate MCMC simulations for constraining parameters in both model. We also plan to further look into the degeneracy in the Runaway Dilaton couplings. On the other hand, the unconstrained mass in BSBM is an interesting phenomena. We plan to look into the critical mass limit past which the contour blows up. So far in this work, we did not consider the contribution of the scalar field in the expansion of the universe. We can check for self consistency in the expansion of the universe by adding scalar field in Hubble parameter. We can also induce an effect like lensing and constrain it using α variation.

We can use forecast of CMB S4 likelihood to rerun our Monte Carlo simulations to predict how better these models will be constrained by the next generation CMB experiment. We can also analyze spatial variation of α with the numerical tools we used for this work.

VI.   CODE REPOSITORY

All code written for this work can be found in the this github repository: `https://github.com/htohfa/Fine-Structure-Constant-Variation`. For solving the differential equations, we use fourth order Runge-kutta method, and emcee package for running MCMC chains.

VII.   ACKNOWLEDGEMENTS

and present my work at the APS April Meeting 2022.

---

[1] Planck Collaboration: N. Aghanim, Y. Akrami, M. Ashdown, J. Aumont, C. Baccigalupi, M. Ballardini, A. J. Banday, R. B. Barreiro, N. Bartolo, S. Basak, R. Battye, K. Benabed, J.-P. Bernard, M. Bersanelli, P. Bielewicz, J. J. Bock, J. R. Bond, J. Borrill, F. R. Bouchet, F. Boulanger, M. Bucher, C. Burigana, R. C. Butler, E. Calabrese, J.-F. Cardoso, J. Carron, A. Challinor, H. C. Chiang, J. Chluba, L. P. L. Colombo, C. Combet, D. Contreras, B. P. Crill, F. Cuttaia, P. de Bernardis, G. de Zotti, J. Delabrouille, J.-M. Delouis, E. Di Valentino, J. M. Diego, O. Doré , M. Douspis, A. Ducout, X. Dupac, S. Dusini, G. Efstathiou, F. Elsner, T. A. Enßlin, H. K. Eriksen, Y. Fantaye, M. Farhang, J. Fergusson, R. Fernandez-Cobos, F. Finelli, F. Forastieri, M. Frailis, A. A. Fraisse, E. Franceschi, A. Frolov, S. Galeotta, S. Galli, K. Ganga, R. T. Génova-Santos, M. Gerbino, T. Ghosh, J. González-Nuevo, K. M. Górski, S. Gratton, A. Gruppuso, J. E. Gudmundsson, J. Hamann, W. Handley, F. K. Hansen, D. Herranz, S. R. Hildebrandt, E. Hivon, Z. Huang, A. H. Jaffe, W. C. Jones, A. Karakci, E. Keihänen, R. Keskitalo, K. Kiiveri, J. Kim, T. S. Kisner, L. Knox, N. Krachmalnicoff, M. Kunz, H. Kurki-Suonio, G. Lagache, J.-M. Lamarre, A. Lasenby, M. Lattanzi, C. R. Lawrence, M. Le Jeune, P. Lemos, J. Lesgourgues, F. Levrier, A. Lewis, M. Liguori, P. B. Lilje, M. Lilley, V. Lindholm, M. López-Caniego, P. M. Lubin, Y.-Z. Ma, J. F. Macías-Pérez, G. Maggio, D. Maino, N. Mandolesi, A. Mangilli, A. Marcos-Caballero, M. Maris, P. G. Martin, M. Martinelli, E. Martínez-González, S. Matarrese, N. Mauri, J. D. McEwen, P. R. Meinhold, A. Melchiorri, A. Mennella, M. Migliaccio, M. Millea, S. Mitra, M.-A. Miville-Deschênes, D. Molinari, L. Montier, G. Morgante, A. Moss, P. Natoli, H. U. Nørgaard-Nielsen, L. Pagano, D. Paoletti, B. Partridge, G. Patanchon, H. V. Peiris, F. Perrotta, V. Pettorino, F. Piacentini, L. Polastri, G. Polenta, J.-L. Puget, J. P. Rachen, M. Reinecke, M. Remazeilles, A. Renzi, G. Rocha, C. Rosset, G. Roudier, J. A. Rubiño-Martín, B. Ruiz-Granados, L. Salvati, M. Sandri, M. Savelainen, D. Scott, E. P. S. Shellard, C. Sirignano, G. Sirri, L. D. Spencer, R. Sunyaev, A.-S. Suur-Uski, J. A. Tauber, D. Tavagnacco, M. Tenti, L. Toffolatti, M. Tomasi, T. Trombetti, L. Valenziano, J. Valiviita, B. Van Tent, L. Vibert, P. Vielva, F. Villa, N. Vittorio, B. D. Wandelt, I. K. Wehus, M. White, S. D. M. White, A. Zacchei, and A. Zonca. iplanck/i 2018 results. *Astronomy &amp Astrophysics*, 641:A6, sep 2020.

[2] Jacob D. Bekenstein. Fine-structure constant: Is it really a constant? *Phys. Rev. D*, 25:1527–1539, Mar 1982.

[3] Jacob D. Bekenstein. Fine-structure constant variability, equivalence principle, and cosmology. *Physical Review D*, 66(12), dec 2002.

[4] Ph. Brax, C. van de Bruck, A. C. Davis, and C. S. Rhodes. Varying Constants in Brane World Scenarios. , 283(4):627–632, January 2003.

[5] Clare Burrage and Jeremy Sakstein. Tests of chameleon gravity. *Living Reviews in Relativity*, 21(1), mar 2018.

[6] Sebastien Clesse. An introduction to inflation after planck: from theory to observations, 2015.

[7] T. Damour, F. Piazza, and G. Veneziano. Violations of the equivalence principle in a dilaton-runaway scenario. *Phys. Rev. D*, 66:046007, Aug 2002.

[8] T. Damour and A.M. Polyakov. The string dilation and a least coupling principle. *Nuclear Physics B*, 423(2-3):532–558, jul 1994.

[9] Thibault Damour and Freeman Dyson. The oklo bound on the time variation of the fine-structure constant revisited. *Nuclear Physics B*, 480(1-2):37–54, nov 1996.

[10] Thibault Damour and Kenneth Nordtvedt. General relativity as a cosmological attractor of tensor-scalar theories. *Phys. Rev. Lett.*, 70:2217–2219, Apr 1993.

[11] Thibault Damour, Federico Piazza, and Gabriele Veneziano. Runaway dilaton and equivalence principle ... - cds.cern.ch.

[12] P. A. M. Dirac. The Cosmological Constants. *Nature (London)*, 139(3512):323, February 1937.

[13] Daniel Foreman-Mackey, David W. Hogg, Dustin Lang, and Jonathan Goodman. ttemcee/tt: The MCMC hammer. *Publications of the Astronomical Society of the Pacific*, 125(925):306–312, mar 2013.

[14] Joshua A. Frieman, Christopher T. Hill, Albert Stebbins, and Ioav Waga. Cosmology with Ultralight Pseudo Nambu-Goldstone Bosons. *Phys. Rev. Lett.*, 75(11):2077–2080, September 1995.

[15] Joshua A. Frieman, Michael S. Turner, and Dragan Huterer. Dark energy and the accelerating universe. *Annual Review of Astronomy and Astrophysics*, 46(1):385–432, sep 2008.

[16] Daniel Grin and Christopher M. Hirata. Cosmological hydrogen recombination: The effect of extremely high-mml:math xmlns:mml="http://www.w3.org/1998/math/MathML"

display="inline"mml:min/mml:mi/mml:mathstates. *Physical Review D*, 81(8), apr 2010.

[17] Luke Hart and Jens Chluba. New constraints on time-dependent variations of fundamental constants using planck data. *Monthly Notices of the Royal Astronomical Society*, 474(2):1850–1861, oct 2017.

[18] Luke Hart and Jens Chluba. Updated fundamental constant constraints from planck 2018 data and possible relations to the hubble tension. *Monthly Notices of the Royal Astronomical Society*, 493(3):3255–3263, feb 2020.

[19] Alireza Hojjati, Levon Pogosian, Alessandra Silvestri, and Gong-Bo Zhao. Observable physical modes of modified gravity. *Physical Review D*, 89(8), mar 2014.

[20] Alireza Hojjati, Gong-Bo Zhao, Levon Pogosian, Alessandra Silvestri, Robert Crittenden, and Kazuya Koyama. Cosmological tests of general relativity: A principal component analysis. *Physical Review D*, 85(4), feb 2012.

[21] Wayne Hu and Scott Dodelson. Cosmic microwave background anisotropies. *Annual Review of Astronomy and Astrophysics*, 40(1):171–216, sep 2002.

[22] Wayne Hu and Naoshi Sugiyama. Anisotropies in the Cosmic Microwave Background: an Analytic Approach. *Astrophys. J.*, 444:489, May 1995.

[23] TH. KALUZA. On the unification problem in physics. *International Journal of Modern Physics D*, 27(14):1870001, oct 2018.

[24] Julian A. King, John K. Webb, Michael T. Murphy, Victor V. Flambaum, Robert F. Carswell, Matthew B. Bainbridge, Michael R. Wilczynska, and F. Elliott Koch. Spatial variation in the fine-structure constant - new results from VLT/UVES. *Monthly Notices of the Royal Astronomical Society*, 422(4):3370–3414, apr 2012.

[25] Oskar Klein. Quantentheorie und fnfdimensionale relativittstheorie. *Zeitschrift fr Physik*, 37(12):895–906, 1926.

[26] M. Kowalski, D. Rubin, G. Aldering, R. J. Agostinho, A. Amadon, R. Amanullah, C. Balland, K. Barbary, G. Blanc, P. J. Challis, A. Conley, N. V. Connolly, R. Covarrubias, K. S. Dawson, S. E. Deustua, R. Ellis, S. Fabbro, V. Fadeyev, X. Fan, B. Farris, G. Folatelli, B. L. Frye, G. Garavini, E. L. Gates, L. Germany, G. Goldhaber, B. Goldman, A. Goobar, D. E. Groom, J. Haissinski, D. Hardin, I. Hook, S. Kent, A. G. Kim, R. A. Knop, C. Lidman, E. V. Linder, J. Mendez, J. Meyers, G. J. Miller, M. Moniez, A. M. Mourão, H. Newberg, S. Nobili, P. E. Nugent, R. Pain, O. Perdereau, S. Perlmutter, M. M. Phillips, V. Prasad, R. Quimby,

N. Regnault, J. Rich, E. P. Rubenstein, P. Ruiz-Lapuente, F. D. Santos, B. E. Schaefer, R. A. Schommer, R. C. Smith, A. M. Soderberg, A. L. Spadafora, L. G. Strolger, M. Strovink, N. B. Suntzeff, N. Suzuki, R. C. Thomas, N. A. Walton, L. Wang, W. M. Wood-Vasey, and J. L. Yun. Improved Cosmological Constraints from New, Old, and Combined Supernova Data Sets. *Astrophys. J.*, 686(2):749–778, October 2008.

[27] W. J. Marciano. Time variation of the fundamental 'constants' and Kaluza-Klein theories. *Phys. Rev. Lett.*, 52:489–491, February 1984.

[28] C. J. A. P. Martins and L. Vacher. Astrophysical and local constraints on string theory: Runaway dilaton models. *Physical Review D*, 100(12), dec 2019.

[29] D. F. Mota. Variations of the fine structure constant in space and time, 2004.

[30] M. T. Murphy, J. K. Webb, and V. V. Flambaum. Further evidence for a variable fine-structure constant from keck/HIRES QSO absorption spectra. *Monthly Notices of the Royal Astronomical Society*, 345(2):609–638, oct 2003.

[31] Lior Pachter. What is principal component analysis?

[32] G. A. Palma, Ph. Brax, A. C. Davis, and C. van de Bruck. Gauge coupling variation in brane models. *Physical Review D*, 68(12), dec 2003.

[33] Dmitri Pogosyan.

[34] Adam G. Riess, Lucas M. Macri, Samantha L. Hoffmann, Dan Scolnic, Stefano Casertano, Alexei V. Filippenko, Brad E. Tucker, Mark J. Reid, David O. Jones, Jeffrey M. Silverman, Ryan Chornock, Peter Challis, Wenlong Yuan, Peter J. Brown, and Ryan J. Foley. A 2.4% Determination of the Local Value of the Hubble Constant. *Astrophys. J.*, 826(1):56, July 2016.

[35] Håvard Bunes Sandvik, John D. Barrow, and Joã o Magueijo. A simple cosmology with a varying fine structure constant. *Physical Review Letters*, 88(3), jan 2002.

[36] A. Songaila and L. L. Cowie. CONSTRAINING THE VARIATION OF THE FINE-STRUCTURE CONSTANT WITH OBSERVATIONS OF NARROW QUASAR ABSORPTION LINES. *The Astrophysical Journal*, 793(2):103, sep 2014.

[37] Jean-Philippe Uzan. The fundamental constants and their variation: observational and theoretical status. *Rev. Mod. Phys.*, 75:403–455, Apr 2003.

[38] J. K. Webb, J. A. King, M. T. Murphy, V. V. Flambaum, R. F. Carswell, and M. B. Bainbridge. Indications of a spatial variation of the fine structure constant. *Physical Review Letters*, 107(19), oct 2011.

[39] John K. Webb, Victor V. Flambaum, Christopher W. Churchill, Michael J. Drinkwater, and John D. Barrow. Search for time variation of the fine structure constant. *Physical Review Letters*, 82(5):884–887, feb 1999.

[40] C. Wetterich. Cosmology and the fate of dilatation symmetry. *Nuclear Physics B*, 302(4):668–696, June 1988.

[41] Ivaylo Zlatev, Limin Wang, and Paul J. Steinhardt. Quintessence, cosmic coincidence, and the cosmological constant. *Physical Review Letters*, 82(5):896–899, feb 1999.